ISSN 0965-5441, Petroleum Chemistry, 2021, Vol. 61, No. 8, pp. 871–874. © Pleiades Publishing, Ltd., 2021.
Russian Text © The Author(s), 2021, published in Sovremennye Molekulyarnye Sita. Advanced Molecular Sieves.

Effect of Metal Cations on the Microstructure of Sol-Gel-Synthesized Silica

E. A. Tarasenko[a] and O. E. Lebedeva[a,*]

[a] *Belgorod State National Research University, Belgorod, 308015 Russia*
**e-mail: OLebedeva@bsu.edu.ru*

Received April 20, 2021; revised May 27, 2021; accepted June 3, 2021

Abstract—The effect of small doping additions (ten metal cations) on the structural characteristics of the sol-gel-synthesized silicas was evaluated by the SAXS method. Doping with cobalt, cerium, and silver cations led to separation of metal compounds as single phases. All the tested cations affected the radius of gyration and the fractal dimension of the resultant silicas.

Keywords: sol-gel synthesis, silica, dopant cations, fractal dimension

DOI: 10.1134/S0965544121080077

Silica-based materials are extensively used in various industry sectors, since, depending on the nature of the components, they acquire specific mechanical, heat-insulating, acoustic, and photoluminescent properties. Silica particles provide a matrix for preparation of catalysts and photocatalysts [1–8]. Silica-based sorbents, whose study has continued for more than half a century, also remain in high demand. Of special interest is controlled synthesis of silica systems by the sol-gel route which allows the properties of materials, in particular their structure and texture, to be fairly easily regulated at the molecular level via changing the synthesis parameters.

Sol-gel synthesis of silicate materials has been the subject of numerous studies whose number is steadily increasing [9–13]. The most common precursor for the preparation of such materials is orthosilicic acid tetraethyl ester (tetraethoxysilane, TEOS). Of critical importance for the structure of the resultant materials is pH of the medium for TEOS hydrolysis. Synthesis in an alkaline medium gives particles with a nearly spherical shape. Hydrolysis in a strongly acidic medium (pH 1–2) yields hierarchically organized three-dimensional branched structures from fractal clusters. Supposedly, synthesis in the metastable and least studied region of pH 1–2 [14–15] may be significantly affected by minor impacts.

Herein, we examined the structural features of the products of TEOS hydrolysis and polycondensation in the presence of small amounts of salts of ten metal cations that significantly differed in charge, size, and electronic structure.

EXPERIMENTAL

High purity grade TEOS [$Si(C_2H_5O)_4$] was used as a precursor for the preparation of silica. As dopants served cations of different metals, whose sources were sodium, potassium, and silver nitrates and crystallohydrates of magnesium, cobalt(II), nickel(II), iron(III), aluminum(III), cerium(III), and lanthanum(III) nitrates. All the chemicals were used without further purification.

Hydrolysis of TEOS was carried out in an aqueous-alcoholic solution at pH = 1–2. A nitric acid solution was used as a hydrolysis catalyst. The reaction mixture components were taken in the molar ratio TEOS : C_2H_5OH : H_2O : HNO_3 = 1 : 4 : 16 : 0.6. For the preparation of doped silica, to aqueous solutions of the corresponding metal salts the required volumes of TEOS, ethanol, and water were added. The resultant transparent colorless or weakly colored gels underwent thermal decomposition in a muffle furnace in air at 600°C for 2 h in order to remove organic synthesis products.

The content of the metal cations in each sample was 3×10^{-4} mol per gram of air-dried doped silica.

X-ray phase analysis was performed with a Rigaku Ultima IV X-ray diffractometer using CuK_α radiation at

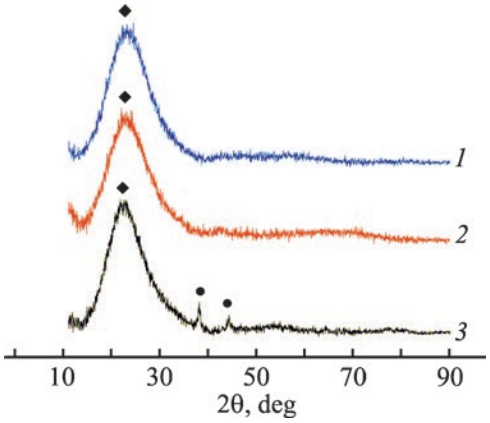

Fig. 1. X-ray powder diffraction pattern of the samples of silica doped with (1) Fe^{3+}, (2) Ce^{3+}, and (3) Ag^{+} cations. (♦) SiO_2 phase and (•) Ag phase.

2θ between 5° and 70° with a step 0.02° at a scan speed 2°/min.

The structure of the doped silicas was analyzed by small-angle X-ray scattering method. The measurements were carried out at the SAXS BioMUR beamline of the Kurchatov synchrotron radiation source using a Pilatus 3 1M detector from Dectris in the (0.04–1.7) nm^{-1} range of scattered vectors. A Si(111) single-crystal focusing monochromator (wavelength of 0.1445 nm) was used. The scattered properties were interpreted in terms of the radius of gyration R_g and the fractal dimension.

TEM micrographs were obtained on a JEOL JEM-2100 microscope at an operating voltage of 200 kV.

RESULTS AND DISCUSSION

The X-ray powder diffraction patterns of all the samples exhibit similar broad peaks in the 2θ range 10°–30° (Fig. 1), which confirms the presence of an X-ray amorphous phase of silica. Only the diffraction pattern of the silver cation-doped silica sample additionally contains reflections attributable to metallic silver. For the Ce^{3+}- and Co^{2+}-doped silica samples the electron microdiffraction patterns revealed the presence of crystalline phases (Fig. 2), but the corresponding crystal lattice parameters could not be determined with sufficient accuracy. Thus, the samples of silicates doped with Ag^{+}, Ce^{3+}, and Co^{2+} cations appeared as amorphous structures of silica with inclusions of the crystalline phase of the corresponding oxide or metal (Ag), i.e., were nanocomposites. In all other cases the metal ions could be incorporated into silicon-oxygen structures as metal-oxygen tetrahedra (triply charged cations) or could form silicates (singly and doubly charged cations), or the content of the phase comprising the metal compounds was less than the limit of detection. The TEM examination of the silica particles morphology confirms the amorphous character of seven samples studied.

Previously [16], we examined the fractal structure of gels produced by hydrolytic polycondensation of

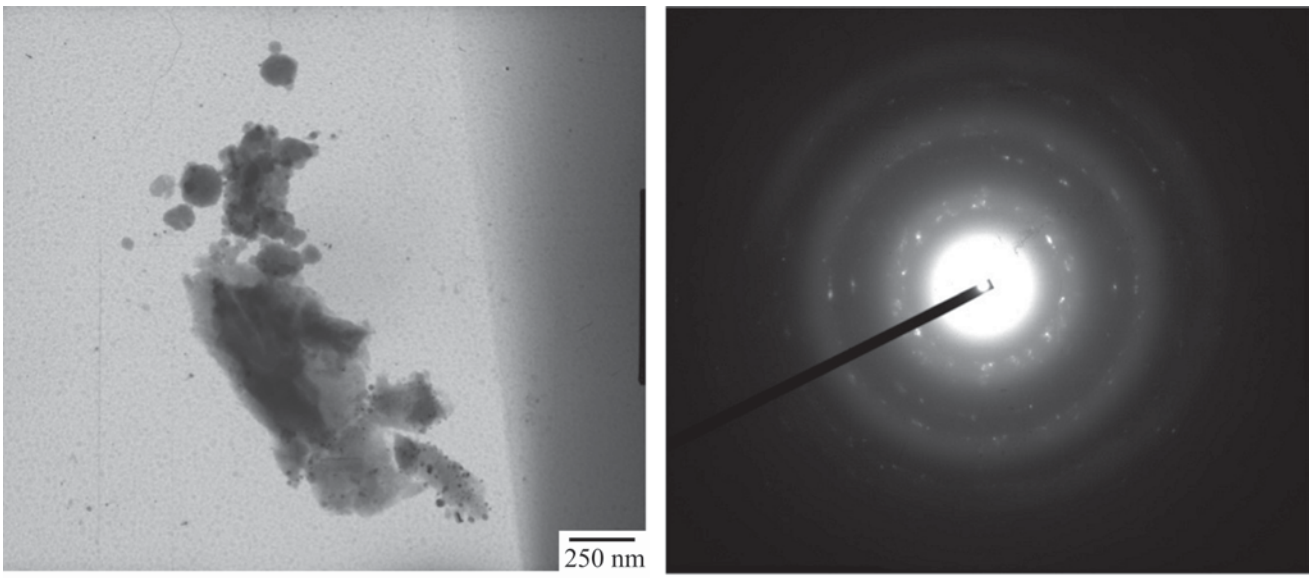

Fig. 2. TEM image and electron microdiffraction pattern of the Ag^{+}-doped silica sample.

Table 1. Structural characteristics of the doped silicas

Dopant cation	–	K^+	Na^+	Ag^+	Mg^{2+}	Co^{2+}	Ni^{2+}	Al^{3+}	Fe^{3+}	Ce^{3+}	La^{3+}
R_g, nm (±0.1 nm)	4.1	11.7	4.7	5.1	3.7	4.1	3.3	4.5	4.4	3.5	3.3
Fractal dimension	2.0	1.0	2.1	2.1	2.4	2.8	2.9	2.3	2.0	2.6	2.6
Fractal type[a]	D_m	D_m	D_s	D_s	D_m	D_m	D_m	D_m	D_m	D_m	D_m

[a] D_m is mass fractal, and D_s, surface fractal.

tetraethoxysilane in the presence of dopant metal cations and found that the gels were mass fractal aggregates. It was natural to assume that the hierarchical fractal organization was retained in the micro- and mesostructures of the resultant xerogels and silica powders, despite a sharp decrease in the average particle size due to collapse of the three-dimensional gel structure, water evaporation, and ethanol burnout, caused by heat treatment. For examination of the fractal structure of the silicas the SAXS method was employed.

Figure 3 shows typical small-angle X-ray scattering curves of the silica powders, and Table 1 presents their structural characteristics. The radius of gyration R_g was determined from the slope of the linear extrapolation of the initial portion of the SAXS curve (Guinier region) plotted as ln I vs. s^2. Knowledge of R_g allows judging the compactness of the scattering aggregate. For a given volume, R_g will be the smallest for the particles with a close to spherical shape, and more anisometric particles will be characterized by a larger radius of gyration. The fractal dimension was calculated using the slope of the tangent to the scattering intensity curve plotted as log I vs. log s in the Porod region. The fractal dimension D_f in the $2 < D_f < 3$ range corresponded to mass fractals. Samples with $D_f > 3$ were attributed to surface fractals, and the fractal dimension was calculated using the relationship $D_s = |6–D_f|$.

The effect from doping on the radius of gyration of the silica samples varied with the metal cation. Doping with magnesium, nickel, cerium, and lanthanum cations led to reduction in the radius of gyration compared to the undoped silica. The presence of cobalt ion did not affect the radius of gyration, which is quite explicable due to the occurrence of the cobalt compound as a single phase. Significant increase in the radius of gyration was caused by doping with potassium. It is worth mentioning that this singly charged cation is not incorporated into the silicon-oxygen chains; presumably, it may hinder the growth of the fractal aggregates. Of all the singly charged cations tested the potassium ion has the largest radius, which may be responsible to a certain extent for its peculiar behavior.

Our results show that most of the silicas studied belong to mass fractals with the fractal dimensions ranging from of 2.1 to 2.9, characteristic of branched three-dimensional structures. Among all the samples studied, those doped with nickel cations had the highest fractal dimension corresponding to the most compact structure. As known, a transition from three-dimensional networks to compact particles with a rough surface occurs at $D_m \geq 3$. We did not record such fractal dimensions, but that of the nickel-containing sample was close enough to this level. Interestingly, formation of structures corresponding to surface fractals was observed in two cases, specifically, for the silicas doped with singly charged sodium and silver cations. A possible reason is that, since singly charged cations cannot be incorporated into the silica microstructure, they may hinder the growth of fractals, as mentioned above.

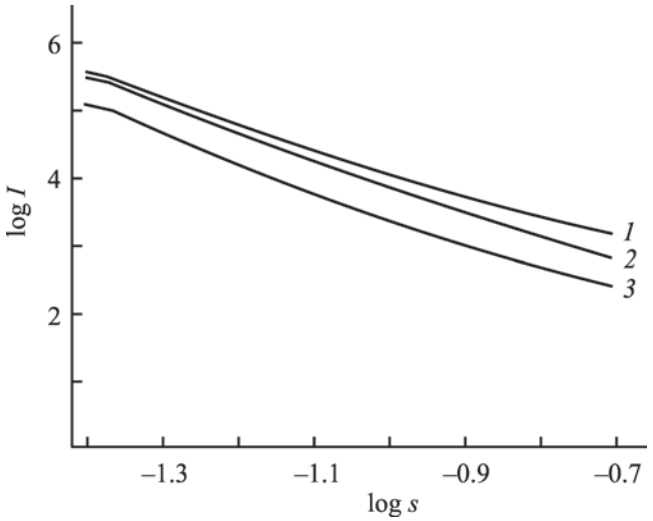

Fig. 3. SAXS curves for the samples of the powders of (*1*, *2*) silicas doped with (*1*) Ag^+ and (*2*) Fe^{3+} cations and (*3*) undoped silica.

Importantly, the effects observed in this study were produced by very small amounts of metal cations introduced into the system during the sol-gel synthesis process. These effects were obviously manifested predominantly in the initial stage of the synthesis, when primary clusters, whose growth was driven by their interaction with each other, were formed from the homogeneous system simultaneously with TEOS hydrolysis. The relationship between the fractal dimension and the model of formation of fractal aggregates was demonstrated in [17]. Specifically, at the fractal dimension within $2 < D_m < 3$ the growth of the aggregates is described by the model of kinetically controlled cluster-cluster or particle-cluster aggregation.

CONCLUSIONS

Thus, doping additions of metal cations introduced during the synthesis process affect the microstructure of silica via altering the radius of gyration and the fractal dimension of the aggregates constituting the material. Double- and triple-charged cations participate in the formation of mass fractals, while single-charged cations cause a change from mass to surface fractal aggregates.

AUTHOR INFORMATION

E.A. Tarasenko, ORCID: http://orcid.org/0000-0003-2094-1337

O.E. Lebedeva, ORCID: http://orcid.org/0000-0002-5021-028X

ACKNOWLEDGMENTS

We are grateful to A.A. Veligzhanin, Head of Department, National Research Center “Kurchatov Institute,” for the assistance in carrying out SAXS analysis of the samples.

CONFLICT OF INTEREST

The authors declare that they have no conflicts of interest requiring disclosure in this article.

REFERENCES

1. Feng, H., Xu, H., Feng, H., Gao, Y., and Jin, X., *Chem. Phys. Lett*., 2019, vol. 733, Article 16676. https://doi.org/10.1016/j.cplett.2019.136676
2. Nithya Deva Krupa, A. and Vimala, R., *Mater. Sci. Eng., C*., 2016, vol. 61, pp. 728–735. https://doi.org/10.1016/j.msec.2016.01.013
3. Ortiz, W.G.C., Delgado, D., Fajardo, C.A.G., Agouram, S., Sanchís, R., Solsona, B., and Nieto, J.M.L., *Mol. Catal*., 2020, vol. 491, Article 110982. https://doi.org/10.1016/j.mcat.2020.110982
4. Neelam, D.M., Jaydeep, A., Burg, A., Shamir, D., and Albo, Y., *Catal. Commun*., 2020, vol. 133, Article 105819. https://doi.org/10.1016/j.catcom.2019.105819
5. Xie, Y.-T., Chen, J.-R., Chen, Y.-T., Jiang, B.-C., Sie, Z.-H., Hsu, H.-Y., Chen, T.-L., Chiang, Y.-Y., and Hsueh, H.-Y., *Chem. Eng. J*., 2021, vol. 405, Article 126572. https://doi.org/10.1016/j.cej.2020.126572
6. Ye, R.-P., Liao, L., Reina, T.R., Liu, J., Chevella, D., Jin, Y., Fan, M., and Liu, J., *Fuel*, 2021, vol. 285, Article 119151. https://doi.org/10.1016/j.fuel.2020.119151
7. Bernardes, A.A., Scheffler, G.L., Radtke, C., Pozebon, D., dos Santos, J.H.Z., and da Rocha, Z.N., *Colloid. Surf., A*, 2020, vol. 584, Article 124020. https://doi.org/10.1016/j.colsurfa.2019.124020
8. Su, Ch., DeHart, T., Anderson, M., and McGinn, P.J., *Mater. Lett*., 2019, vol. 234, pp. 168–171. https://doi.org/10.1016/j.matlet.2018.09.093
9. Dolinina, E.S., Kraev, A.S., and Parfenyuk, E.V., *Mendeleev Commun*., 2020, vol. 30, no. 6, pp. 812–814. https://doi.org/10.1016/j.mencom.2020.11.041
10. Diktanaitė, A., Gaidamavičienė, G., Kazakevičius, E., Kežionis, A., and Žalga, A., *Thermochim. Acta*, 2020, vol. 685, Article 178511. https://doi.org/10.1016/j.tca.2020.178511
11. Ling, F.W.M., Abdulbari, H.A., and Chin, S.-Y., *Mater. Today: Proc*., 2021, vol. 42, pp. 1–7. https://doi.org/10.1016/j.matpr.2020.07.563
12. Raghunandan, S., Suresh Kumar, R., Kamaraj, M., and Gandhi, A.S., *Ceram. Int*., 2019, vol. 45, pp. 4487–4492. https://doi.org/10.1016/j.ceramint.2018.11.129
13. Babiarczuk, B., Lewandowski, D., Szczurek, A., Kierzek, K., Meffert, M., Gerthsen, D., Kaleta, J., and Krzak, J., *J. Supercrit. Fluid*, 2020, vol. 166, Article 104997. https://doi.org/10.1016/j.supflu.2020.104997
14. Iler, R.K., *The Chemistry of Silica: Solubility, Polymerization, Colloid and Surface Properties, and Biochemistry of Silica*, New York: Wiley and Sons, 1979.
15. Levy, D. and Zayat, M., *The Sol-Gel Handbook*, New York: Wiley and Sons, 2015. https://doi.org/10.1002/9783527670819
16. Tarasenko, E., Lebedeva, O., Peters, G., and Veligzhanin, A., *Russ. J. Phys. Chem. A*, 2019, vol. 93, pp. 1737–1740. https://doi.org/10.1134/S0036024419090279
17. Roldugin, V.I., *Russ. Chem. Rev*., 2003, vol. 72, no. 10, pp. 823–848. https://doi.org/10.1070/RC2003v072n10ABEH000805